Available online at www.eccomasproceedia.org
Eccomas Proceedia UNCECOMP (2025) 240-252

ECCOMAS
Proceedia

UNCECOMP 2025
6th ECCOMAS Thematic Conference on
Uncertainty Quantification in Computational Science and Engineering
M. Papadrakakis, V. Papadopoulos, G. Stefanou (eds.)
Rhodes Island, Greece, 15-18 June 2025

A GENERALIZED CONTACT POINT RESPONSE ESTIMATION VIA ON-BOARD SENSING

Ho Man Siu[1], **Elias G. Dimitrakopoulos**[1], **Costas Papadimitriou**[2]

[1]The Hong Kong University of Science and Technology
Department of Civil and Environmental Engineering
Clear Water Bay, Kowloon, Hong Kong, China
e-mail: hmsiu@connect.ust.hk, ilias@ust.hk

[2]University of Thessaly
Department of Mechanical Engineering
Pedion Areos, Volos 38334
e-mail: costasp@uth.gr

Abstract. *This work aims to present a generalized approach for estimating contact point acceleration response using only vehicle measurement, assuming the parameter of the vehicle model is known. The estimated contact point response is useful in identifying the frequencies of the passing bridge since the contact point response is free of vehicle frequency. To solve the input-state estimation problem involved, we employ an Augmented Kalman Filter (AKF). This work presents proof of concept utilizing a simplified single-degree-of-freedom (SDOF) and a more realistic multi-degree-of-freedom (MDOF) vehicle model, both representing typical road vehicles. Meanwhile, we model the bridge as a simply supported beam with the finite element method. This analysis provides valuable insight into the effect of different parameters on the accuracy of contact point response. Our demonstration relies on simulated data from a highway bridge-vehicle interaction model, incorporating the impact of road roughness.*

Keywords: On-board sensing, bridges, input-state estimation, frequency estimation, contact point response.

ISSN:2623-3339
Peer-review under responsibility of the organizing committee of UNCECOMP 2025.
doi: 10.7712/120225.12353.21130

1 INTRODUCTION

The modal properties of a bridge often reflec the state of structural health. Therefore, monitoring the changes in modal properties can facilitate proper maintenance action. Conventionally, engineers rely on sensors mounted at different locations on the target bridge [1] to estimate modal frequencies. Although numerous studies have shown the robustness and efficien y of these direct methods [2, 3, 4, 5, 6], such techniques often come with significan installation, labor, and maintenance expenses. Importantly, this type of approach suffers from the restriction of "one-system-per bridge", hence it is challenging to meet the growing demand for bridge structural health monitoring.

Alternatively, indirect approaches, a.k.a. vehicle scanning methods, have proliferated in the bridge structural health monitoring fiel in the past several decades, since such methods enable the monitoring of multiple bridges with one instrumented test vehicle. Yang et al. [7] firs proposed the concept of extracting bridge frequencies from the response of a single-degree-of-freedom (SDOF) vehicle traversing the bridge and demonstrated its feasibility experimentally [8]. Subsequent studies have explored estimating frequencies and modal shapes from vehicle acceleration measurements using various signal processing techniques, including time-frequency domain decomposition [9], continuous wavelet transform [10], Hilbert-Huang transform [11], and two-peak spectrum idealized filte [12].

Although extracting bridge modal information from vehicle responses is feasible, vehicle frequencies often overlap with bridge frequencies in the vehicle response spectrum, complicating the identificatio process. To overcome this challenge, using the contact point response of the scanning vehicle helps mitigate vehicle frequency interference [13, 14, 15]. Utilizing this property of the contact point signal, recent studies proposed various signal processing techniques for the extraction of bridge frequencies [16], damping ratios [16], and mode shapes [13, 15]. Nevertheless, road roughness can still obscure the bridge signal if the bridge response is weak. To tackle this issue, recent studies have utilized the concept that vehicle wheels traverse the same road roughness at different times, focusing on residual vehicle contact point signals. Jin et al. [17, 18, 19] suggested the application of subspace identificatio techniques on the residual vehicle contact point signal to estimate bridge frequencies. Meanwhile, Yang et al. [20, 21, 22] proposed the use of residual contact point acceleration alongside signal processing to obtain bridge modal properties.

Directly measuring contact point response presents challenges due to the lack of appropriate sensors. Thus, inferring contact point response from vehicle measurements becomes necessary. Most studies have employed analytical approaches to back-calculate the contact point acceleration of vehicles. However, the analytical expressions for back-calculating contact point acceleration vary with the types of vehicle models [13, 14, 15, 16, 20, 21, 22, 23, 24]. Instead of relying on the analytical expression to back-calculate the contact point response, the fiel has also adopted Bayesian inference techniques to infer the contact point signal. In particular, the application of the Bayesian expectation-maximization algorithm has been suggested to estimate the contact point displacement [25]. Building on the idea of using the Bayesian filterin technique, this study introduces a new state-space formulation that relates contact point acceleration to the fl xible modal response of the vehicle. Based on the proposed state-space model, we estimate contact point acceleration using an Augmented Kalman Filter (AKF) [26, 27].

2 VEHICLE BRIDGE SYSTEM MODELING

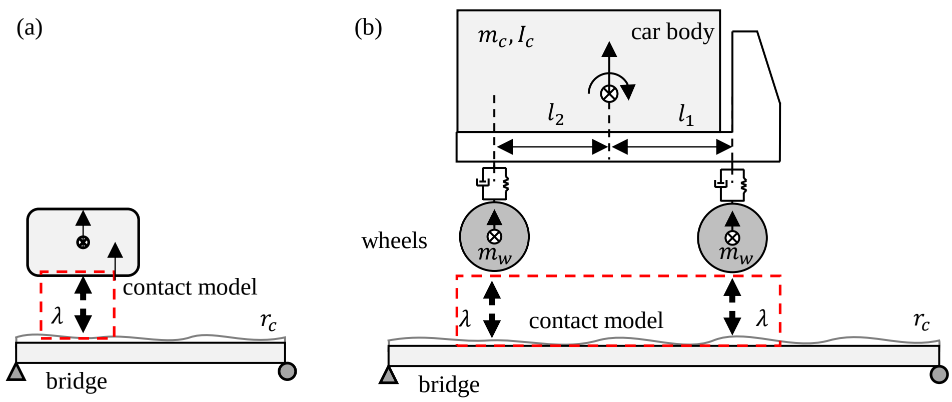

Figure 1: (a) SDOF (b) MDOF vehicle model on a bridge.

The equation of motion (EOM) of the vehicle sub-system can take the form:

$$\mathbf{m}_v \ddot{\mathbf{u}}_v(t) + \mathbf{c}_v \dot{\mathbf{u}}_v(t) + \mathbf{k}_v \mathbf{u}_v(t) - \mathbf{W}_v \boldsymbol{\lambda}(t) = \mathbf{f}_v \tag{1}$$

where, $\mathbf{u}_v(t)$ is the displacement vector of the vehicle and $\mathbf{m}_v$, $\mathbf{c}_v$, $\mathbf{k}_v$ are, respectively, the mass, damping, and stiffness matrices of the vehicle (where subscript $()_v$ denotes the vehicle subsystem). $\mathbf{W}_v$ is a contact direction matrix of the vehicle, which maps the contact forces to the wheels' DOFs [28, 29, 30, 31].

Similar to the vehicle subsystem, the EOM of the bridge about its (statically) deformed configuratio under its self-weight is:

$$\mathbf{m}_b \ddot{\mathbf{u}}_b(t) + \mathbf{c}_b \dot{\mathbf{u}}_b(t) + \mathbf{k}_b \mathbf{u}_b(t) + \mathbf{W}_b \boldsymbol{\lambda}(t) = \mathbf{W}_b \mathbf{f}_{wv} \tag{2}$$

with $\mathbf{u}_b(t)$ being the displacement vector of the bridge and $\mathbf{m}_b$, $\mathbf{c}_b$, and $\mathbf{k}_b$ being the mass, damping, and stiffness matrices of the bridge (subscript $()_b$ denotes the bridge subsystem). $\mathbf{W}_b$ is the contact direction matrix of the bridge that maps the contact force $\boldsymbol{\lambda}$ and the vehicle weight $\mathbf{f}_{wv}$ to the appropriate DOFs of the bridge [28, 29, 30, 31].

Combining Eqs. (1) and (2), the EOM of the coupled vehicle-bridge system becomes:

$$\mathbf{M}\ddot{\mathbf{u}}(t) + \mathbf{C}\dot{\mathbf{u}}(t) + \mathbf{K}\mathbf{u}(t) + \mathbf{W}_c \boldsymbol{\lambda}(t) = \mathbf{f} \tag{3}$$

where, $\mathbf{u}$ is the displacement vector of the whole system and $\mathbf{M}$, $\mathbf{C}$, and $\mathbf{K}$ are, respectively, the mass, damping, and stiffness matrices of the whole system:

$$\mathbf{M} = \begin{bmatrix} \mathbf{m}_v & \mathbf{0} \\ \mathbf{0} & \mathbf{m}_b \end{bmatrix}, \mathbf{C} = \begin{bmatrix} \mathbf{c}_v & \mathbf{0} \\ \mathbf{0} & \mathbf{c}_b \end{bmatrix}, \mathbf{K} = \begin{bmatrix} \mathbf{k}_v & \mathbf{0} \\ \mathbf{0} & \mathbf{k}_b \end{bmatrix} \tag{4}$$

and $\mathbf{W}_c = \left[-\mathbf{W}_v{}^{\mathrm{T}} \quad \mathbf{W}_b{}^{\mathrm{T}}\right]^{\mathrm{T}}$ is the contact direction matrix of the coupled system.

In this study, we assume a compliance contact model consisting of a spring and a damper connected in parallel between the wheel and the bridge. Accordingly, the contact force acting on the i^{th} wheel λ_i has the following expression: [29, 32].

$$\lambda_i(t) = k_{\lambda,i}\left(-u_{w,i} + u_{cp,i}\right) + c_{\lambda,i}\left(-\dot{u}_{w,i} + \dot{u}_{cp,i}\right) \tag{5}$$

where $k_{\lambda,i}$ and $c_{\lambda,i}$ are the contact stiffness and damping coefficien respectively, and $u_{w,i}$ is the displacement of the i^{th} wheel. The contact point response (displacement $u_{cp,i}$, velocity $\dot{u}_{cp,i}$ and acceleration $\ddot{u}_{cp,i}$) has the following expression:

$$u_{cp,i} = \mathbf{W}_{b,i}^{\mathrm{T}}(x_i)\mathbf{u}_b(t) + r_c(x_i) \tag{6}$$

$$\dot{u}_{cp,i} = \mathbf{W}_{b,i}^{\mathrm{T}}(x_i)\dot{\mathbf{u}}_b(t) + v\mathbf{W}'^{\mathrm{T}}_{b,i}(x_i)\mathbf{u}_b(t) + v{r_c}'(x_i) \tag{7}$$

$$\ddot{u}_{cp,i} = \mathbf{W}_{b,i}^{\mathrm{T}}(x_i)\ddot{\mathbf{u}}_b(t) + 2v\mathbf{W}'^{\mathrm{T}}_{b,i}(x_i)\dot{\mathbf{u}}_b(t) + v^2\mathbf{W}''^{\mathrm{T}}_{b,i}(x_i)\mathbf{u}_b(t) + v^2{r_c}''(x_i) \tag{8}$$

where r_c is the road roughness and $\mathbf{W}_{b,i}$ is the i^{th} column of $\mathbf{W}_b$. The prime ($\square'$) denotes the derivative with respect to the space variable x.

We model the road roughness (Figure 2) as stationary stochastic processes using the spectral representation method [33]. and adopt the road roughness parameters from ISO 8606:2016 [34].

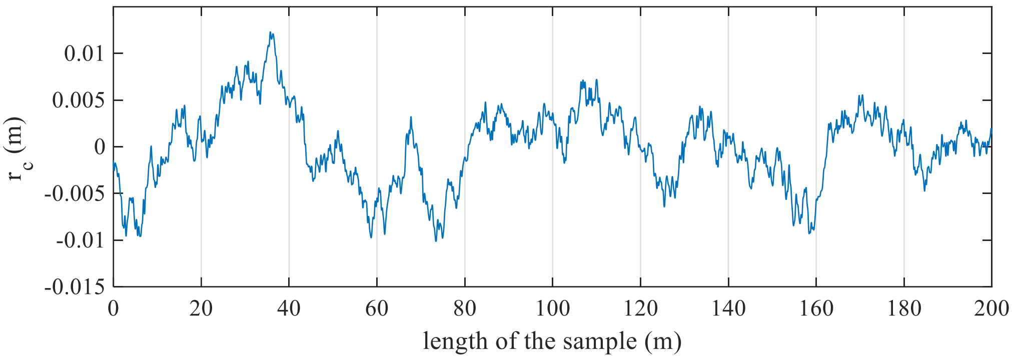

Figure 2: Sample of class A road roughness profile according to ISO8606 [34].

3 Contact point response estimation

The contact point response and the vehicle response are connected. To study this, we consider a modifie vehicle system (see Figure 3), where the vehicle model includes additional DOFs with small mass that remain in continuous contact with the bridge/ road surface. This approach works because the compliance contact model represents a special case of a rigid contact model with a small (close to zero) contact mass.

3.1 Modal analysis of the modified vehicle

The previous study [27] demonstrates the feasibility of estimating contact force using the state-space model of fl xible mode dynamics. By introducing a partitioned mass-normalized mode shape matrix of the modifie vehicle system:

$$\mathbf{\Phi}_v = \left[\mathbf{\Phi}_{rigid} \quad \mathbf{\Phi}_{flex}\right] \tag{9}$$

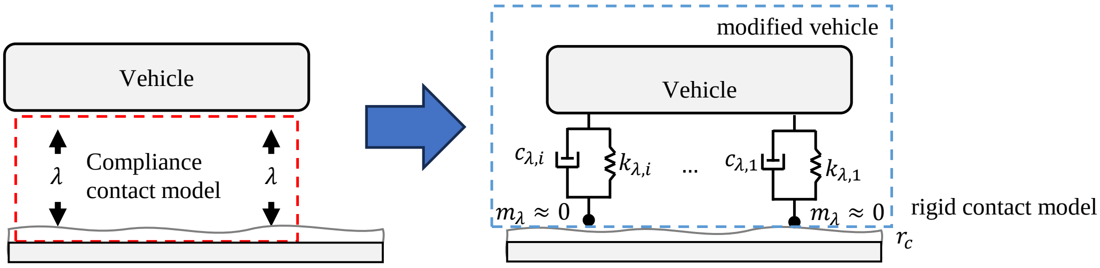

Figure 3: Modificatio of vehicle model.

where matrix $\mathbf{\Phi}$ comprises all m_0 rigid body mode shape(s) (mode(s) with zero eigenfrequency) $\mathbf{\Phi}_{rigid}$ and all m_f fl xible mode shape(s) $\mathbf{\Phi}_{flex}$ (where $m_f = m - m_0$), the relationship between the physical and modal coordinates of the modifie vehicle is:

$$\mathbf{u}_v(t) = \mathbf{\Phi}_v \boldsymbol{\xi}_v \tag{10}$$

where $\boldsymbol{\xi}_v(t)$ represents the modal displacement vector. One can partition the modal displacement vector into two parts:

$$\boldsymbol{\xi}_v = \left[\boldsymbol{\xi}_{rigid}^{\mathrm{T}} \quad \boldsymbol{\xi}_{flex}^{\mathrm{T}}\right]^{\mathrm{T}} \tag{11}$$

where $\boldsymbol{\xi}_{rigid}$ is the modal displacement of the rigid body mode(s) and $\boldsymbol{\xi}_{flex}$ is the modal displacement of the fl xible modes. Substituting Eq. (10) into Eq. (1) and pre-multiplying both sides by $\mathbf{\Phi}^{\mathrm{T}}$ yields the EOM of the modifie vehicle in modal coordinates:

$$\ddot{\boldsymbol{\xi}}_{rigid} = \mathbf{\Phi}_{rigid}^{\mathrm{T}} \mathbf{W}_v \boldsymbol{\lambda}(t) \tag{12}$$

$$\ddot{\boldsymbol{\xi}}_{flex} + \mathbf{Z}_{flex}\dot{\boldsymbol{\xi}}_{flex} + \mathbf{\Lambda}_{flex}\boldsymbol{\xi}_{flex} = \mathbf{\Phi}_{flex}^{\mathrm{T}} \mathbf{W}_v \boldsymbol{\lambda}(t) \tag{13}$$

with $\mathbf{Z}_{flex} = \mathbf{\Phi}_{flex}^{\mathrm{T}} \mathbf{c}_v \mathbf{\Phi}_{flex}$ and $\mathbf{\Lambda}_{flex} = \mathbf{\Phi}_{flex}^{\mathrm{T}} \mathbf{k}_v \mathbf{\Phi}_{flex}$.

From the equation above, we can express the vehicle displacement and acceleration as follows:

$$\mathbf{u}_v = \mathbf{u}_{v,rigid} + \mathbf{u}_{v,flex} = \mathbf{\Phi}_{rigid}\boldsymbol{\xi}_{rigid} + \mathbf{\Phi}_{flex}\boldsymbol{\xi}_{flex} \tag{14}$$

$$\ddot{\mathbf{u}}_v = \left[\mathbf{\Phi}_{rigid}\mathbf{\Phi}_{rigid}^{T} + \mathbf{\Phi}_{flex}\mathbf{\Phi}_{flex}^{\mathrm{T}}\right] \mathbf{W}_v \boldsymbol{\lambda}(t) - \mathbf{\Phi}_{flex}\mathbf{\Lambda}_{flex}\boldsymbol{\xi}_{flex} - \mathbf{\Phi}_{flex}\mathbf{Z}_{flex}\dot{\boldsymbol{\xi}}_{flex} \tag{15}$$

where $\mathbf{u}_{v,rigid}$ and $\mathbf{u}_{v,flex}$ are the contribution of the rigid body and fl xible modes in vehicle displacement, respectively.

Then, we can derive the following relationship between the contact point acceleration and contact force:

$$\ddot{\mathbf{u}}_{cp} = \mathbf{W}_v^{\mathrm{T}}\ddot{\mathbf{u}}_v = \mathbf{W}_v^{\mathrm{T}}\mathbf{\Phi}\mathbf{\Phi}^{\mathrm{T}}\mathbf{W}_v\boldsymbol{\lambda}(t) - \mathbf{W}_v^{\mathrm{T}}\mathbf{\Phi}_{flex}\mathbf{Z}_{flex}\dot{\boldsymbol{\xi}}_{flex} - \mathbf{W}_v^{\mathrm{T}}\mathbf{\Phi}_{flex}\mathbf{\Lambda}_{flex}\boldsymbol{\xi}_{flex} \tag{16}$$

$$\boldsymbol{\lambda}(t) = \left(\mathbf{W}_v^{\mathrm{T}}\mathbf{\Phi}\mathbf{\Phi}^{\mathrm{T}}\mathbf{W}_v\right)^{-1}\left(\ddot{\mathbf{u}}_{cp} + \mathbf{W}_v^{\mathrm{T}}\mathbf{\Phi}_{flex}\mathbf{Z}_{flex}\dot{\boldsymbol{\xi}}_{flex} + \mathbf{W}_v^{\mathrm{T}}\mathbf{\Phi}_{flex}\mathbf{\Lambda}_{flex}\boldsymbol{\xi}_{flex}\right) \tag{17}$$

Substituting Eq. (17) into Eq. (12) and (13) yields the modal EOM of the vehicle with contact point acceleration $\ddot{\mathbf{u}}_{cp}$ as input:

$$\ddot{\boldsymbol{\xi}}_{rigid} = \mathbf{\Phi}_{rigid}^{\mathrm{T}}\mathbf{W}_v\left(\mathbf{W}_v^{\mathrm{T}}\mathbf{\Phi}\mathbf{\Phi}^{\mathrm{T}}\mathbf{W}_v\right)^{-1}\left(\ddot{\mathbf{u}}_{cp} + \mathbf{W}_v^{\mathrm{T}}\mathbf{\Phi}_{flex}\mathbf{Z}_{flex}\dot{\boldsymbol{\xi}}_{flex} + \mathbf{W}_v^{\mathrm{T}}\mathbf{\Phi}_{flex}\mathbf{\Lambda}_{flex}\boldsymbol{\xi}_{flex}\right) \tag{18}$$

$$\ddot{\boldsymbol{\xi}}_{flex} = \boldsymbol{\Phi}_{flex}^{\mathrm{T}} \mathbf{W}_v \left(\mathbf{W}_v^{\mathrm{T}} \boldsymbol{\Phi} \boldsymbol{\Phi}^{\mathrm{T}} \mathbf{W}_v \right)^{-1} \left(\ddot{\mathbf{u}}_{cp} + \mathbf{W}_v^{\mathrm{T}} \boldsymbol{\Phi}_{flex} \mathbf{Z}_{flex} \dot{\boldsymbol{\xi}}_{flex} + \mathbf{W}_v^{\mathrm{T}} \boldsymbol{\Phi}_{flex} \boldsymbol{\Lambda}_{flex} \boldsymbol{\xi}_{flex} \right) - \mathbf{Z}_{flex} \dot{\boldsymbol{\xi}}_{flex} - \boldsymbol{\Lambda}_{flex} \boldsymbol{\xi}_{flex} \tag{19}$$

From Eqs. (18) and (19), we can express the vehicle acceleration in term of $\ddot{\mathbf{u}}_{cp}$, $\dot{\boldsymbol{\xi}}_{flex}$ and $\boldsymbol{\xi}_{flex}$ as:

$$\ddot{\mathbf{u}}_v = \boldsymbol{\Phi}\boldsymbol{\Phi}^{\mathrm{T}} \mathbf{W}_v \left(\mathbf{W}_v^{\mathrm{T}} \boldsymbol{\Phi} \boldsymbol{\Phi}^{\mathrm{T}} \mathbf{W}_v \right)^{-1} \ddot{\mathbf{u}}_{cp} + \left(\boldsymbol{\Phi}\boldsymbol{\Phi}^{\mathrm{T}} \mathbf{W}_v \left(\mathbf{W}_v^{\mathrm{T}} \boldsymbol{\Phi} \boldsymbol{\Phi}^{\mathrm{T}} \mathbf{W}_v \right)^{-1} \mathbf{W}_v^{\mathrm{T}} \boldsymbol{\Phi}_{flex} - \boldsymbol{\Phi}_{flex} \right) \mathbf{Z}_{flex} \dot{\boldsymbol{\xi}}_{flex} + \left(\boldsymbol{\Phi}\boldsymbol{\Phi}^{\mathrm{T}} \mathbf{W}_v \left(\mathbf{W}_v^{\mathrm{T}} \boldsymbol{\Phi} \boldsymbol{\Phi}^{\mathrm{T}} \mathbf{W}_v \right)^{-1} \mathbf{W}_v^{\mathrm{T}} \boldsymbol{\Phi}_{flex} - \boldsymbol{\Phi}_{flex} \right) \boldsymbol{\Lambda}_{flex} \boldsymbol{\xi}_{flex} \tag{20}$$

and the strain at the suspension springs as:

$$\varepsilon(t) = \boldsymbol{\Psi} \mathbf{u}_v(t) = \boldsymbol{\Psi} \boldsymbol{\Phi}_{flex} \boldsymbol{\xi}_{flex}(t) \tag{21}$$

where $\boldsymbol{\Psi}$ is the matrix that associates the displacements at all DOFs to the strains at the springs of the train vehicle model.

3.2 State-space model of the vehicle with contact point acceleration as input

The state-space form of the modal EOM for the modifie vehicle model (Eq. (13)) is: [35]:

$$\dot{\mathbf{x}}(t) = \mathbf{A}_c \mathbf{x}(t) + \mathbf{B}_c \ddot{\mathbf{u}}_{cp}(t) \tag{22}$$

where the state vector $\mathbf{x}(t)$, state matrix $\mathbf{A}_c$ and the input matrix $\mathbf{B}_c$ are:

$$\mathbf{x}(t) = \begin{bmatrix} \boldsymbol{\xi}_{flex} \\ \dot{\boldsymbol{\xi}}_{flex} \end{bmatrix}, \quad \mathbf{A}_c = \begin{bmatrix} \mathbf{0} & \mathbf{I} \\ \mathbf{I}_{flex} \boldsymbol{\Lambda}_{flex} & \mathbf{I}_{flex} \mathbf{Z}_{flex} \end{bmatrix}, \quad \mathbf{B}_c = \begin{bmatrix} \mathbf{0} \\ \boldsymbol{\Phi}_{flex}^{\mathrm{T}} \mathbf{W}_v \left(\mathbf{W}_v^{\mathrm{T}} \boldsymbol{\Phi} \boldsymbol{\Phi}^{\mathrm{T}} \mathbf{W}_v \right)^{-1} \end{bmatrix} \tag{23}$$

$$\mathbf{I}_{flex} = \left(\boldsymbol{\Phi}_{flex}^{\mathrm{T}} \mathbf{W}_v \left(\mathbf{W}_v^{\mathrm{T}} \boldsymbol{\Phi} \boldsymbol{\Phi}^{\mathrm{T}} \mathbf{W}_v \right)^{-1} \mathbf{W}_v^{\mathrm{T}} \boldsymbol{\Phi}_{flex} - \mathbf{I} \right) \tag{24}$$

The observation equation for accelerations and strain measurements is:

$$\mathbf{y}(t) = \mathbf{G}\mathbf{x}(t) + \mathbf{J}\ddot{\mathbf{u}}_{cp}(t) + \mathbf{v}(t) \tag{25}$$

where $\mathbf{y}(t)$ is the measurement vector in continuous time, the measurement noise is white, i.e., $\mathbf{v} \sim \mathcal{N}(\mathbf{0}, \mathbf{Q}_y)$, with measurement error covariance $\mathbf{Q}_y \in \mathbb{R}^{N_O \times N_O}$ and N_O is the number of measured quantities. From Eqs. (20) and (21), $\mathbf{G}$ and $\mathbf{J}$ matrices for acceleration and strain measurements it follows:

$$\mathbf{G} = \begin{bmatrix} \mathbf{H}\mathbf{I}_{mod} \boldsymbol{\Lambda}_{flex} & \mathbf{H}\mathbf{I}_{mod} \mathbf{Z}_{flex} \\ \mathbf{S}\boldsymbol{\Psi}\boldsymbol{\Phi}_{flex} & \mathbf{0} \end{bmatrix}, \quad \mathbf{J} = \begin{bmatrix} \mathbf{H}\boldsymbol{\Phi}\boldsymbol{\Phi}^{\mathrm{T}} \mathbf{W}_v \left(\mathbf{W}_v^{\mathrm{T}} \boldsymbol{\Phi} \boldsymbol{\Phi}^{\mathrm{T}} \mathbf{W}_v \right)^{-1} \\ \mathbf{0} \end{bmatrix}, \tag{26}$$

where

$$\mathbf{I}_{mod} = \left(\boldsymbol{\Phi}\boldsymbol{\Phi}^{\mathrm{T}} \mathbf{W}_v \left(\mathbf{W}_v^{\mathrm{T}} \boldsymbol{\Phi} \boldsymbol{\Phi}^{\mathrm{T}} \mathbf{W}_v \right)^{-1} \mathbf{W}_v^{\mathrm{T}} \boldsymbol{\Phi}_{flex} - \boldsymbol{\Phi}_{flex} \right) \tag{27}$$

In practice, we take vehicle measurements at discrete time instant $t_k = k\Delta t$, where k is the time step and Δt is the sampling time interval. Hence, it is necessary to discretize the vehicle state-space model. Using the Tustin method [36], we can express the discrete state-space form of the EOM for the vehicle as:

$$\mathbf{x}_{k+1} = \mathbf{A}_d\mathbf{x}_k + \mathbf{B}_d\ddot{\mathbf{u}}_{cp,k} + \mathbf{w}_k \tag{28}$$

$$\mathbf{y}_k = \mathbf{G}_d\mathbf{x}_k + \mathbf{J}_d\ddot{\mathbf{u}}_{cp,k} + \mathbf{v}_k \tag{29}$$

where the value of the state-space vector and the contact point acceleration at time instant t_k are $\mathbf{x}_k$ and $\ddot{\mathbf{u}}_{cp,k}$, respectively ($\mathbf{x}_k \equiv \mathbf{x}(k\Delta t)$ and $\ddot{\mathbf{u}}_{cp,k} \equiv \ddot{\mathbf{u}}_{cp}(k\Delta t)$). We assume the process noise $\mathbf{w}_k$ is zero-mean Gaussian, i.e., $\mathbf{w}_k \sim \mathcal{N}(\mathbf{0}, \mathbf{Q}_x)$ with process noise covariance $\mathbf{Q}_x \in \mathbb{R}^{2m_f \times 2m_f}$.

3.3 AKF for unknown contact point acceleration estimation

This study employs a random walk model [26, 27] to describe the changes in the unknown contact point acceleration $\ddot{\mathbf{u}}_{cp,k}$ at different time steps:

$$\ddot{\mathbf{u}}_{cp,k+1} = \ddot{\mathbf{u}}_{cp,k} + \boldsymbol{\eta}_k \tag{30}$$

where $\boldsymbol{\eta}_k \sim \mathcal{N}(\mathbf{0}, \mathbf{Q}_\lambda)$ is a zero-mean Gaussian with covariance matrix $\mathbf{Q}_\lambda \in \mathbb{R}^{n_\lambda \times n_\lambda}$. By introducing the augmented state vector $\mathbf{x}_k^a = [\mathbf{x}_k^{\mathrm{T}}, \ddot{\mathbf{u}}_{cp,k}^{\mathrm{T}}]^{\mathrm{T}}$, the augmented state-space model and observation equations are formulated as follows:

$$\begin{aligned} \mathbf{x}_{k+1}^a &= \mathbf{A}^a\mathbf{x}_k^a + \boldsymbol{\zeta}_k \\ \mathbf{y}_k &= \mathbf{G}^a\mathbf{x}_k^a + \mathbf{v}_k \end{aligned} \tag{31}$$

where the augmented system matrix $\mathbf{A}^a \in \mathbb{R}^{(2m_f+n_\lambda)\times(2m_f+n_\lambda)}$ and observation matrix $\mathbf{G}^a \in \mathbb{R}^{N_0\times(2m_f+n_\lambda)}$ are:

$$\mathbf{A}^a = \begin{bmatrix} \mathbf{A}_d & \mathbf{B}_d \\ \mathbf{0} & \mathbf{I} \end{bmatrix}, \quad \mathbf{G}^a = \begin{bmatrix} \mathbf{G}_d & \mathbf{J}_d \end{bmatrix} \tag{32}$$

The augmented process noise $\boldsymbol{\zeta}_k \sim \mathcal{N}(\mathbf{0}, \mathbf{Q}_a)$ has a covariance matrix $\mathbf{Q}_a \in \mathbb{R}^{(m_f+n_\lambda)\times(m_f+n_\lambda)}$:

$$\mathbf{Q}_a = \begin{bmatrix} \mathbf{Q}_x & \mathbf{0} \\ \mathbf{0} & \mathbf{Q}_\lambda \end{bmatrix} \tag{33}$$

Using a Kalman Filtering algorithm [26, 27, 35], we can obtain the estimated augmented state $\hat{\mathbf{x}}_{k|k}^a$, which contains the contact point acceleration of interest. The algorithm involves a time update:

$$\begin{aligned} \hat{\mathbf{x}}_{k|k-1}^a &= \mathbf{A}^a\hat{\mathbf{x}}_{k-1|k-1}^a \\ \mathbf{P}_{k|k-1} &= \mathbf{A}^a\mathbf{P}_{k-1|k-1}(\mathbf{A}^a)^{\mathrm{T}} + \mathbf{Q}_a \end{aligned} \tag{34}$$

and a measurement update:

$$\begin{aligned} \mathbf{K}_k &= \mathbf{P}_{k|k-1}(\mathbf{G}^a)^{\mathrm{T}}(\mathbf{G}^a\mathbf{P}_{k|k-1}(\mathbf{G}^a)^{\mathrm{T}} + \mathbf{Q}_y)^{-1} \\ \hat{\mathbf{x}}_{k|k}^a &= \hat{\mathbf{x}}_{k|k-1}^a + \mathbf{K}_k(\mathbf{y}_k - \mathbf{G}^a\hat{\mathbf{x}}_{k|k-1}^a) \\ \mathbf{P}_{k|k} &= \mathbf{P}_{k|k-1} - \mathbf{K}_k\mathbf{G}^a\mathbf{P}_{k|k-1} \end{aligned} \tag{35}$$

for every time step.

4 NUMERICAL EXAMPLES

To evaluate the performance of the proposed Augmented Kalman Filter (AKF), we employ simulated data from bridge-vehicle interaction model. In the following examples, the vehicle enters the bridge at $t = 5$s and moves along a simply supported bridge modeled with Euler-Bernoulli beams element. The bridge is 30 m long with mass per unit length 36t/m, fl xural rigidity $EI = 205\text{GNm}^2$, and the damping ratio of the bridge is $\zeta_b = 2\%$ [17].

4.1 SDOF vehicle

To verify the proposed method, this section studies a simplifie SDOF vehicle (as illustrated in Figure 1(a)) moving across the bridge with constant speed $v = 72\text{km/h}$. The SDOF vehicle has a mass of $m_c = 5.75\text{t}$, with a suspension featuring a stiffness coefficien $k_p = 1.595\text{MN/m}$ and a damping coefficien $c_p = 3.20\text{kN/m}$. We assume a road roughness profil of class A [34].

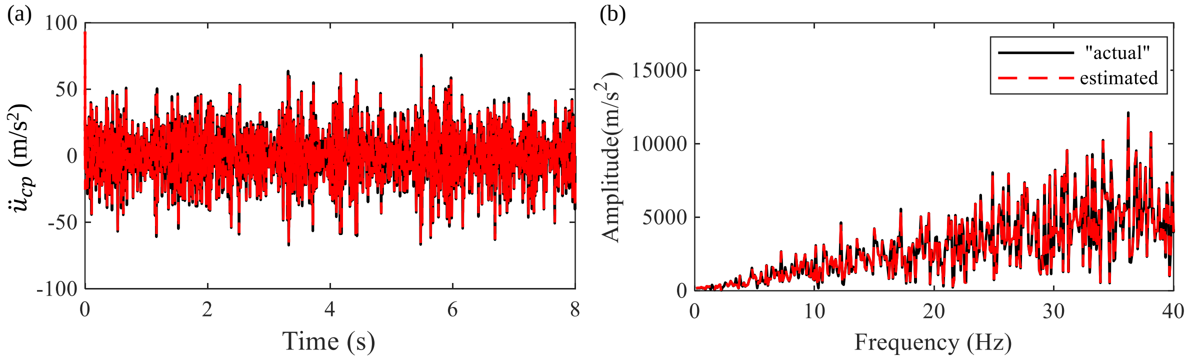

Figure 4: Comparison between the “actual” and estimated contact point acceleration using acceleration measurement of the car body: (a) time history; (b) Fourier spectrum ($v = 72\text{km/h}$).

Figure 4 compares the “actual” and estimated contact point acceleration based on acceleration measurements of the vehicle body. Throughout this study, the term “actual” refers to the response obtained from vehicle-bridge simulation. The estimated contact point acceleration and the corresponding spectrum closely match the “actual” contact point acceleration when there is no measurement noise. This demonstrates the effectiveness of the proposed state-space model and AKF in accurately estimating the unknown contact point acceleration.

4.2 2 axles MDOF vehicle

The section examines a more realistic 2-axles MDOFs truck vehicle (Figure 1(b)) moving at a constant speed $v = 72\text{km/h}$. The road roughness profil remains the same. Table 1 shows the mechanical properties of the vehicle [37].

Table 1: Mechanical properties of the 2 axles MDOF vehicle

m_c (t)	I_c (tm^2)	m_{w1} (t)	m_{w2} (t)	k (kN/m)	c (kNs/m)	k_λ (kN/m)	c_λ (kNs/m)	l_1 (m)	l_2 (m)
4.48	5.52	0.8	0.71	798	46.42	702	1.6	2.6	3

Figure 5 compares the “actual” and estimated contact point acceleration using acceleration measurement of all DOF and the strain measurements of all the suspension springs. The AKF method effectively captures all high-frequency details of the contact point acceleration. The accuracy of the estimated contact point acceleration for both axles, in both the time and frequency

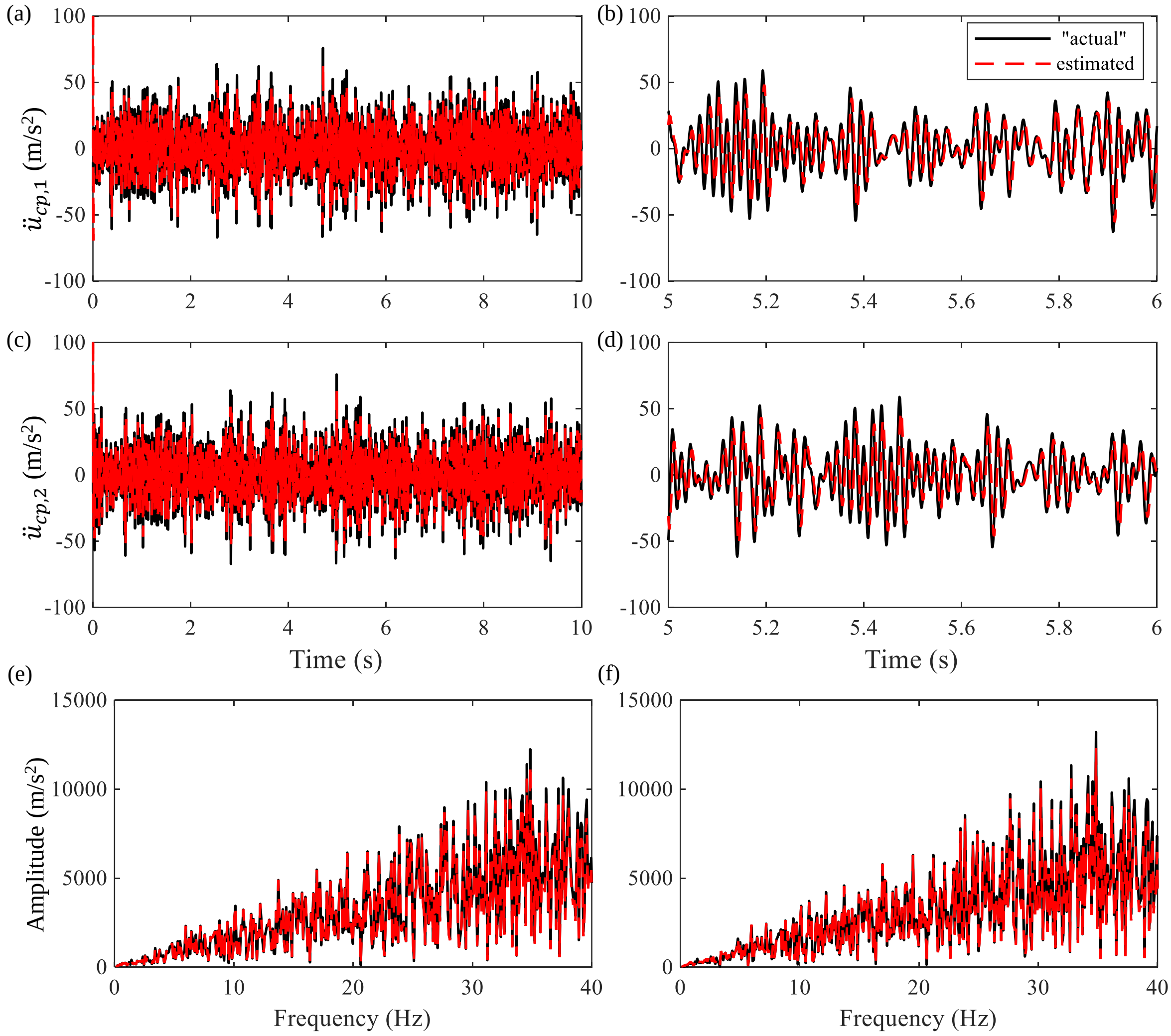

Figure 5: Comparison between the "actual" and estimated contact point acceleration of (a) wheel 1, and (b) wheel 2 using acceleration measurements at all DOFs and strain measurements of all suspensions (v = 72km/h).

domains, demonstrates the versatility of the proposed state-space formulation. This formulation applies to any vehicle type, making it valuable for real-world applications that require estimating contact point acceleration for various vehicles.

To extract useful information about the passing bridge, such as modal frequencies, from vehicle measurements, numerous studies have shown that the residual contact point response (i.e., acceleration) serves as a better signal for this purpose, as it remains free from the effects of road roughness and vehicle frequency.

Figure 6 illustrates the comparison between the "actual" and estimated residual contact point acceleration. Although a significant error appears in the estimated residual contact point when the vehicle's firs wheel enters (t = 5s) and exits (t = 6.5s) the bridge, the estimated residual contact point acceleration aligns closely with the "actual" values in the time domain. Furthermore, we can observe the firs three modes of the bridge within the spectrum of the estimated residual contact point acceleration. This observation highlights the potential of the proposed formulation to estimate bridge properties using only vehicle measurements.

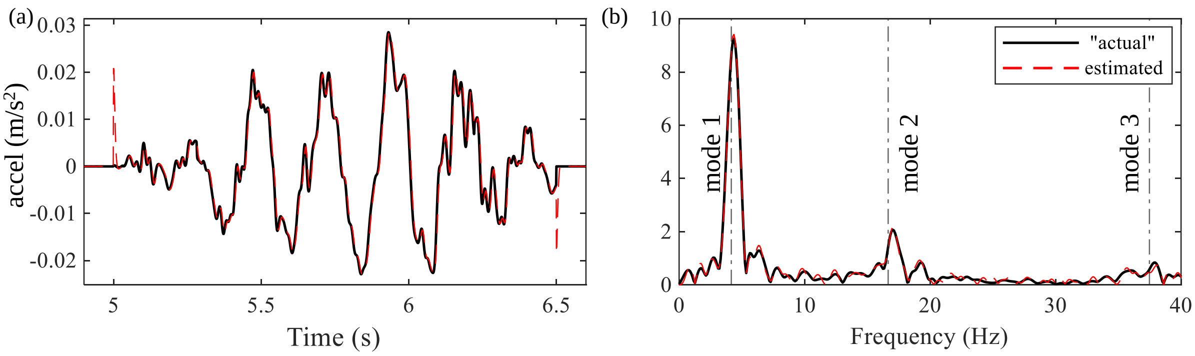

Figure 6: Comparison between the "actual" and estimated residual contact point acceleration: (a) time history; (b) Fourier spectrum

5 CONCLUSIONS

This study explores the feasibility of identifying the vehicle-bridge contact point acceleration using only measurements from on-board sensors installed on vehicles. Specifi ally, it proposes employing the Augmented Kalman Filter (AKF) to identify the unknown contact point acceleration experienced by the passing vehicle. The study assumes a known vehicle model for the vehicle dynamics. Using a mode superposition description of the vehicle dynamics, we remove the influenc of the rigid body mode(s) and formulate a state-space model with contact point acceleration as the input. To demonstrate the effectiveness of the AKF under various conditions, the analysis relies on numerical simulation experiments. The vehicle-bridge simulation examines SDOF and MDOFs vehicle models while considering road roughness. Comparisons between the estimated and "actual" contact point acceleration show that the AKF can achieve high accuracy when properly tuned with suitable covariance settings and sufficien measurement data. The accuracy of the estimated contact point acceleration is adequate for bridge health monitoring purposes.

6 ACKNOWLEDGEMENTS

Financial support to the firs author was provided by the University Grants Committee Research Grants Council of Hong Kong, under Grant Reference Number GRF 16212522.

REFERENCES

[1] Y. An, E. Chatzi, S.-H. Sim, S. Laflamme B. Blachowski, J. Ou, Recent progress and future trends on damage identificatio methods for bridge structures, Structural Control and Health Monitoring 26 (10) (2019) e2416. doi:https://doi.org/10.1002/stc.2416.

[2] C. McGeown, F. Huseynov, D. Hester, P. McGetrick, E. J. O'Brien, V. Pakrashi, Using measured rotation on a beam to detect changes in its structural condition, Journal of Structural Integrity and Maintenance (2021). doi:10.1080/24705314.2021.1906092.

[3] D. Martinez, A. Malekjafarian, E. J. O'Brien, Bridge health monitoring using deflectio measurements under random traffic Structural Control Health Monitoring (2020). doi:10.1002/stc.2593.

[4] Y. Y. Li, Hypersensitivity of strain-based indicators for structural damage identification A review, Mechanical Systems and Signal Processing (2010). doi:10.1016/j.ymssp.2009.11.002.

[5] J.-X. Mao, H. Wang, D.-M. Feng, T.-Y. Tao, W. Zheng, Investigation of dynamic properties of long-span cable-stayed bridges based on one-year monitoring data under normal operating condition, Structural Control Health Monitoring (2018). doi:10.1002/stc.2146.

[6] L. Zhang, E. J. OBrien, D. Hajializadeh, L. Deng, S. Yin, S. Yin, Bridge damage identificatio using rotation measurement, Journal of Bridge Engineering (2023). doi:10.1061/jbenf2.beeng-5891.

[7] Y. Yang, C. W. Lin, J. D. Yau, Extracting bridge frequencies from the dynamic response of a passing vehicle, Journal of Sound and Vibration 272 (3) (2004) 471–493. doi:https://doi.org/10.1016/S0022-460X(03)00378-X.

[8] C. Lin, Y. Yang, Use of a passing vehicle to scan the fundamental bridge frequencies: An experimental verification Engineering Structures 27 (13) (2005) 1865–1878. doi:https://doi.org/10.1016/j.engstruct.2005.06.016.

[9] A. Malekjafarian, E. J. OBrien, Identificatio of bridge mode shapes using short time frequency domain decomposition of the responses measured in a passing vehicle, Engineering Structures 81 (2014) 386–397. doi:https://doi.org/10.1016/j.engstruct.2014.10.007.

[10] E. Erduran, F. M. Pettersen, S. Gonen, A. Lau, Identificatio of vibration frequencies of railway bridges from train-mounted sensors using wavelet transformation, Sensors 23 (3) (2023). doi:10.3390/s23031191.

[11] A. Malekjafarian, E. J. OBrien, On the use of a passing vehicle for the estimation of bridge mode shapes, Journal of Sound and Vibration 397 (2017) 77–91. doi:https://doi.org/10.1016/j.jsv.2017.02.051.

[12] J. Zhou, Z. Lu, Z. Zhou, C. Pan, S. Cao, J. Cheng, J. Zhang, Extraction of bridge mode shapes from the response of a two-axle passing vehicle using a two-peak spectrum idealized filte approach, Mechanical Systems and Signal Processing 190 (2023) 110122. doi:https://doi.org/10.1016/j.ymssp.2023.110122.

[13] Y. B. Yang, Y. H. Liu, H. Xu, Recovering mode shapes of curved bridges by a scanning vehicle, International Journal of Mechanical Sciences 253 (2023) 108404. doi:https://doi.org/10.1016/j.ijmecsci.2023.108404.

[14] H. Xu, Y. H. Liu, Z. L. Wang, K. Shi, B. Zhang, Y. B. Yang, General contact response of single-axle two-mass test vehicles for scanning bridge frequencies considering suspension effect, Engineering Structures 270 (2022) 114880. doi:https://doi.org/10.1016/j.engstruct.2022.114880.

[15] H. Xu, Y. H. Liu, M. Yang, D. S. Yang, Y. B. Yang, Mode shape construction for bridges from contact responses of a two-axle test vehicle by wavelet transform, Mechanical Systems and Signal Processing 195 (2023) 110304. doi:https://doi.org/10.1016/j.ymssp.2023.110304.

[16] Y. B. Yang, K. Shi, Z. L. Wang, H. Xu, B. Zhang, Y. T. Wu, Using a Single-DOF Test Vehicle to Simultaneously Retrieve the First Few Frequencies and Damping Ratios of the Bridge, International Journal of Structural Stability and Dynamics 21 (08) (2021) 2150108. doi:10.1142/S021945542150108X.

[17] N. Jin, Y. B. Yang, E. G. Dimitrakopoulos, T. S. Paraskeva, L. S. Katafygiotis, Application of short-time stochastic subspace identificatio to estimate bridge frequencies from a traversing vehicle, Engineering Structures 230 (2021) 111688. doi:https://doi.org/10.1016/j.engstruct.2020.111688.

[18] N. Jin, V. K. Dertimanis, E. N. Chatzi, E. G. Dimitrakopoulos, L. S. Katafygiotis, Subspace identificatio of bridge dynamics via traversing vehicle measurements, Journal of Sound and Vibration 523 (2022) 116690. doi:https://doi.org/10.1016/j.jsv.2021.116690.

[19] Y. Quan, Q. Zeng, N. Jin, Y. Zhu, C. Liu, Subspace identificatio of bridge frequencies based on the dimensionless response of a two-axle vehicle, Sensors 24 (6) (2024). doi:10.3390/s24061946.

[20] Y. B. Yang, X. Q. Mo, K. Shi, Z. L. Wang, H. Xu, Y. T. Wu, Contact residue for simultaneous removal of vehicle's frequency and surface roughness in scanning bridge frequencies using two connected vehicles, International Journal of Structural Stability and Dynamics 21 (13) (2021) 2171006. doi:10.1142/S0219455421710061.

[21] Y. B. Yang, X. Q. Mo, K. Shi, Z.-L. Wang, H. Xu, Y. T. Wu, Scanning torsional-fl xural frequencies of thin-walled box girders with rough surface from vehicles' residual contact response: Theoretical study, Thin-Walled Structures 169 (2021) 108332. doi:https://doi.org/10.1016/j.tws.2021.108332.

[22] Y. B. Yang, H. Xu, Z.-L. Wang, K. Shi, Using vehicle–bridge contact spectra and residue to scan bridge's modal properties with vehicle frequencies and road roughness eliminated, Structural Control and Health Monitoring 29 (8) (2022) e2968. doi:https://doi.org/10.1002/stc.2968.

[23] Y. Yang, X. Mo, K. Shi, S. Gao, N. Liu, Z. Han, Effect of damping on torsional-fl xural frequencies of monosymmetric thin-walled beams scanned by moving vehicles, Thin-Walled Structures 198 (2024) 111633. doi:https://doi.org/10.1016/j.tws.2024.111633.

[24] B. Wang, Y. Zeng, D. Feng, Theoretical study of extracting modal frequencies and hinge joint stiffness for thin-walled assembled multi-girder bridges from 3d vehicle, Thin-Walled Structures 205 (2024) 112429. doi:https://doi.org/10.1016/j.tws.2024.112429.

[25] J. Li, X. Zhu, S. Chen, W. Ruan, Contact-point response reconstruction for indirect bridge monitoring via bayesian expectation-maximization based augmented kalman filter, Engineering Structures 309 (2024) 118066. doi:https://doi.org/10.1016/j.engstruct.2024.118066.

[26] E. Lourens, E. Reynders, G. De Roeck, G. Degrande, G. Lombaert, An augmented Kalman filte for force identificatio in structural dynamics, Mechanical Systems and Signal Processing 27 (1) (2012) 446–460. doi:10.1016/j.ymssp.2011.09.025.

[27] H. M. Siu, F. Filippitzis, C. D. Stoura, C. Papadimitriou, E. G. Dimitrakopoulos, Utilizing on-board sensing of passing train vehicles for virtual sensing of bridges, Engineering Structures 319 (2024) 118808. doi:https://doi.org/10.1016/j.engstruct.2024.118808.

[28] C. D. Stoura, E. G. Dimitrakopoulos, Additional damping effect on bridges because of vehicle-bridge interaction, Journal of Sound and Vibration 476 (2020) 115294. doi:https://doi.org/10.1016/j.jsv.2020.115294.

[29] C. D. Stoura, E. G. Dimitrakopoulos, MDOF extension of the modifie bridge system method for vehicle–bridge interaction, Nonlinear Dynamics 102 (2020) 2103–2123. doi:10.1007/s11071-020-06022-6.

[30] H. Homaei, E. Dimitrakopoulos, A. Bakhshi, Vehicle-bridge interaction and the tuned-mass damper effect on bridges during vertical earthquake excitation, Acta Mechanica 235 (2024) 1379–1394. doi:10.1007/s00707-023-03533-2.

[31] H. Homaei, C. D. Stoura, E. G. Dimitrakopoulos, Extended modifie bridge system (embs) method for decoupling seismic vehicle-bridge interaction, Earthquake Engineering & Structural Dynamics 53 (13) (2024) 4054–4075. doi:https://doi.org/10.1002/eqe.4209.

[32] E. G. Dimitrakopoulos, Q. Zeng, A three-dimensional dynamic analysis scheme for the interaction between trains and curved railway bridges, Computers & Structures 149 (2015) 43–60. doi:https://doi.org/10.1016/j.compstruc.2014.12.002.

[33] Y.-B. Yang, Z. Yao, Y. S. Wu, Vehicle-bridge interaction dynamics: with applications to high-speed railways, World Scientific River Edge, NJ, 2004.

[34] ISO 8608:2016 Mechanical vibration — Road surface profile — Reporting of measured data, Standard, International Organization for Standardization, Geneva, CH (2016).

[35] D. Simon, Optimal state estimation: Kalman, H_∞, and Nonlinear Approaches, John Wiley & Sons, 2006. doi:10.1002/0470045345.

[36] C. D. Stoura, V. K. Dertimanis, C. Hoelzl, C. Kossmann, A. Cigada, E. N. Chatzi, A Model-Based Bayesian Inference Approach for On-Board Monitoring of Rail Roughness Profiles Application on Field Measurement Data of the Swiss Federal Railways Network, Structural Control and Health Monitoring 2023 (2023) 8855542. doi:10.1155/2023/8855542.

[37] Y. Li, N. Chen, K. Zhao, H. Liao, Seismic response analysis of road vehicle-bridge system for continuous rigid frame bridges with high piers, Earthquake Engineering and Engineering Vibration 11 (2012) 593–602. doi:10.1007/s11803-012-0144-y.